



Cite this: *J. Mater. Chem. B*, 2015, 3, 1831

## Smart electroconductive bioactive ceramics to promote *in situ* electrostimulation of bone

Diogo Mata,<sup>\*a</sup> Filipe J. Oliveira,<sup>a</sup> Miguel A. Neto,<sup>a</sup> Manuel Belmonte,<sup>b</sup> Alexandre C. Bastos,<sup>a</sup> Maria A. Lopes,<sup>c</sup> Pedro S. Gomes,<sup>d</sup> Maria H. Fernandes<sup>d</sup> and Rui F. Silva<sup>a</sup>

Biomaterials can still be reinvented to become simple and universal bone regeneration solutions. Following this roadmap, conductive CNT-based “smart” materials accumulate exciting grafting qualities for tuning the *in vitro* cellular phenotype. Biphasic electrical stimulation of human osteoblastic cells was performed *in vitro* on either dielectric bioactive bone grafts or conductive CNT-reinforced composites. The efficiency of the electrical stimuli delivery, as well as the effect of stimulation on cellular functions were investigated. Conductive substrates boosted the local culture medium conductivity and the confinement of the exogenous electrical fields. Hence, bone cell proliferation, DNA content and mRNA expression were maximized on the conductive substrates yielding superior stimuli delivering efficiency over dielectric ones. These findings are suggestive that bioactive bone grafts with electrical conductivity are capable of high spatial and temporal control of bone cell stimulation.

Received 30th September 2014  
Accepted 8th January 2015

DOI: 10.1039/c4tb01628a

www.rsc.org/MaterialsB

### 1. Introduction

Bone regenerative medicine has undergone huge progress in the past few decades driven by the great socioeconomic interest in treating skeletal diseases.<sup>1</sup> However, there have been tremendous improvements in synthetic bone graft materials, most are still incapable of fully repairing and regenerating severe bone injuries.<sup>2</sup> The development of solutions followed the routes of complex tissue engineering, involving cell manipulation and simpler strategies, such as “smart” bone grafts with new functionalities, capable of stimulating specific phenotype expressions of osteoblastic cells.<sup>2,3</sup> One such exciting functionality is to take advantage of the piezoelectric effect of bone. The forces exerted internally on the bone generate electrical signals that are carried to the bone cells, therefore helping to regulate their biological functions.<sup>4,5</sup> These electrical currents, found in healthy bone, are not expected to exist at the fractured bone site, in case of bone tissue damage or loosening. Thus, it was thought that the use of exogenous electric fields would mimic the mislaid endogenous electric signals and accelerate bone healing.<sup>6</sup>

Electrical stimulation, broadly attained by capacitive coupled electrical field, direct current field and electromagnetic

field has been used to enhance the bone healing process by activating voltage-gated  $\text{Ca}^{2+}$  channels in osteoblast cell plasma membranes.<sup>7–9</sup> The direct application of electric current *in vitro* has been found to induce cell elongation, modulate cell alignment and favor the migration and invasion of human mesenchymal stem cells (hMSCs) into injured sites.<sup>10</sup> Electrical stimulation also seems to enhance cell proliferation and osteogenic differentiation of osteoblastic precursor cells.<sup>11,12</sup> These findings seem to substantiate the improved musculoskeletal healing attained with electrical stimulation in clinical trials aimed at different applications of bone repair/regeneration, which have been reviewed.<sup>13–15</sup>

These data have inspired the development of conductive synthetic matrices to assist in the bone regeneration process under electric stimulation.<sup>16,17</sup> This comes particularly useful because electric/electromagnetic strategies are spatially non-delimited, indiscriminately affecting both target and non-targeting anatomical locations. In the latter, the likely activation of voltage-dependent pathway signals in the surrounding tissues may lead to an overloaded concentration of the internal  $\text{Ca}^{2+}$  concentration in cells causing functional disorders (e.g. oxidative stress, cytotoxicity) and its premature apoptosis.<sup>18,19</sup> Ideally for clinical applications, the electric stimuli should be confined within the tissue volume expected to be regenerated.

The use of metal containing bone grafts in electrical stimulation protocols is precluded due to corrosion phenomenon that induces cytotoxicity.<sup>20</sup> The characteristics of carbon nanotubes (CNTs), namely, the ultimate electrical conductivity in a non-metallic phase and their high aspect-ratio, make them the highest performance filler to obtain highly conductive biomaterials at low

<sup>a</sup>CICECO, Materials and Ceramic Eng. Dept., Univ. of Aveiro, 3810-193 Aveiro, Portugal. E-mail: diogomata@ua.pt; Fax: +351 234 425 300

<sup>b</sup>Institute of Ceramics and Glass, CSIC, 28049 Madrid, Spain

<sup>c</sup>CEMUC, Metallurgical and Materials Eng. Dept., Faculty of Eng., Univ. of Porto, 4200-465 Porto, Portugal

<sup>d</sup>Laboratory for Bone Metabolism and Regeneration, Faculty of Dental Medicine, Univ. of Porto, 4200-465 Porto, Portugal

percolation thresholds without damaging the biological profile of the matrix. While several polymeric matrixes<sup>11,16,21,22</sup> and mesoporous silica<sup>23</sup> have been imparted with CNTs to improve their characteristics, these matrices are essentially non bioactive, and therefore fail to exert an osteoconductive, osteoinductive or osteogenic action within neighboring bone. Ceramic/glass-based substrates may be able to sustain a bioactive profile in contact with the bone and in a process mediated by the CNTs enclosure provide the scaffold material with electrical conductivity. CNTs were used as a mechanical reinforcement of dielectric bone grafts, namely, HA (hydroxyapatite) reinforced composites, proving that the mechanical properties, bioactivity and osteointegration were improved relative to single phase HA even if electrical stimulation was not considered.<sup>24,25</sup> For electrical functionality to be used, the level of CNT individualization should be enough to allow a low electrical percolation threshold and to improve, or at least avoid, the degradation of the mechanical properties relative to those of the matrix. The difficulty in doing this indicates that CNT agglomerates will always be present and that they should be placed within biologically safe diameter sizes (<20  $\mu\text{m}$ ).<sup>26</sup> Nevertheless, their presence insures that the contact area between the CNTs and bone cells will be larger ( $\approx 60 \mu\text{m}$ ) and may also give rise to other functionality. In the bundles there will be cell accessible CNTs with nano-topography that may control cell orientation, migration and also enhance cell adhesion and proliferation.<sup>27,28</sup> Moreover, CNTs in the bundles could be provided with functional groups capable of anchoring bioactive molecules (e.g. bone morphogenic proteins – BMPs) and drugs (e.g. antibiotics) that can be then delivered *in situ* to the fracture site while simultaneously providing electrical stimulation.<sup>29</sup>

The main motivation of the work presented here was to develop and test *in vitro* a CNT/HA/glass composite material with adequate mechanical, electrical, microstructural and, most importantly, biological characteristics, to apply as an electroconductive bone graft. The available literature describes the osteoblastic cell response to electrical stimulation either on non-conductive or conductive substrates. However, comparative studies reporting on the efficiency of stimuli delivered on dielectric and conductive substrates were not found. The use of AC impedance spectroscopy and vibrating voltage probe measurements in  $\alpha$ -MEM (minimal essential medium) reveal the converging effects the conductive composite material has on the electric field and current flow paths. The results for cell viability/proliferation, DNA content and gene expression increase proving that electrical stimulation clearly induced cell growth and differentiation on the electroconductive biocomposite. The results validate the hypothesis that these new biodegradable CNT/HA/glass bone grafts could be used together with a non-invasive electrical stimulation technique to activate cell growth preferentially in the healing zone of the bone.

## 2. Materials and methods

### 2.1. Preparation of the CNT/glass/HA samples

Bioglass (65  $\text{P}_2\text{O}_5$ , 15CaO, 10CaF<sub>2</sub>, 10Na<sub>2</sub>O mol%) and HA powders were lab-prepared from high purity (>98%) grade reagents: the glass was formed at 1450  $^{\circ}\text{C}$  for 90 min in a

platinum crucible, and then rapidly cooled to room temperature; HA was synthesised using a conventional precipitation method.

Commercially available CNTs (NC7000, Nanocyl, Belgium) were used in this work for preparing the composites. The CNTs were purified (>99%) following a non-destructive procedure that involved annealing at 1900  $^{\circ}\text{C}$  for 8 h in a flowing Ar atmosphere. The CNT/glass/HA composite powder suspensions were mixed in isopropyl alcohol using a non-destructive process with volume fractions of 4.4 vol% CNTs, above the electric percolation threshold, and densified by hot pressing at a fixed pressure of 30 MPa for 60 min at 1100  $^{\circ}\text{C}$ . Full description of these processes have been reported previously.<sup>30,31</sup>

### 2.2. Characterization of samples

Microstructural characterization was carried out on polished surfaces of the selected samples by scanning electron microscopy, SEM (Hitachi, SU-70). X-ray diffraction (X'PERT-MPD Philips, CuK $\alpha$ 1 radiation ( $\lambda = 0.154056 \text{ nm}$ ) with a step size of 0.02 $^{\circ}$ ) and Raman spectroscopy (Alpha300 WITec GmbH) were used to identify the different phases present in the glass/HA matrix and in the 4.4 vol% CNTs composite. Raman imaging was performed using an excitation wavelength of 532 nm. For the imaging, 75 points were acquired per line for a total of 75 lines. The scan size was 80  $\times$  80  $\mu\text{m}^2$  and 90 ms of acquisition time per spectrum. Mechanical characterization (biaxial flexural and compressive tests) was carried out using Zwick/Roell Z020 equipment with a load cell of 2.5 kN under a constant displacement rate of 0.3 and 1 mm min<sup>-1</sup>, respectively. The biaxial flexural strength values were measured using a circular plate geometry with 20 mm diameter discs according to ASTM F394-76: the specimen is supported by 3 ball bearings spaced 120 $^{\circ}$  apart on a 13 mm diameter circle. Loading was applied by a cylinder with a flat loading face with 1.0 mm diameter. For compressive strength, a cross head speed of 1.0 mm min<sup>-1</sup> was used for the 2.5  $\times$  2.5  $\times$  4.5 mm<sup>3</sup> samples. Samples of similar dimensions were used to measure the DC electrical conductivity of the glass/HA and CNT/glass/HA materials by fixing copper wires to the smallest faces of the 2.5  $\times$  2.5  $\times$  4.5 mm<sup>3</sup> parallelepipeds. The characterization was performed at room temperature in a Keithley 617 programmable electrometer with the voltage applied in 0.5 V steps over a range of 0–100 V for the dielectric samples. For the conductive samples, a programmable power supply (ISO-TECH IPS-603) was used by applying a voltage over a range of 0–1 V in 0.1 V steps.

### 2.3. Electrical field lines in $\alpha$ -MEM solution

In order to evaluate the effect of the conductive substrates on the electrical behavior of the culture medium used in the cell proliferation studies, the resistance of  $\alpha$ -minimal essential medium ( $\alpha$ -MEM) with different conductive samples (CNT/glass/HA, highly ordered pyrolytic graphite – HOPG and stainless steel 316L – SS316L) was obtained using electrochemical impedance spectroscopy (EIS) on a Autolab PGstat 302N (Eco Chemie, The Netherlands). A two electrode arrangement was used with spiral platinum electrodes with the solution and

conductive samples between them. The impedance of the electrochemical cell was measured in the frequency range of 100 kHz to 10 Hz with 7 points per decade logarithmically distributed; the sinusoidal perturbation was 10 mV rms at an open circuit potential (OCP). The effect of different substrate geometry on the current paths was also assessed by measuring the current lines in solution (12 mL  $\alpha$ -MEM) using a vibrating voltage probe under  $3 \text{ mV cm}^{-1}$  of applied electrical field and a current of 100  $\mu\text{A}$ . The equipment used was manufactured by Applicable Electronics Inc. (USA) and controlled by the ASET 2.0 program developed by Sciencewares (USA). The vibrating microelectrode was a polymer insulated Pt-Ir microwire with a 20  $\mu\text{m}$  diameter platinum black sphere electrodeposited on the tip. The probe vibrates in 2 orthogonal directions ( $X$  and  $Z$ ) and measures the potential difference between the two ends of the vibration. The potential difference divided by the distance between the extremes of vibration gives the local electric field, which can be converted to a local current density by knowing the solution conductivity.<sup>32–34</sup>

#### 2.4. Characterization of the cell stimulation system

A stimulation system was designed to reproduce the *in situ* stimuli conditions delivered by capacitive coupling stimulation used in clinics.<sup>9,35</sup> This system includes three main components: a culture dish electrode assembly (stimulation box, Fig. 1a and b); a function generator; and a PC control interface (Fig. 1a). The stimulation box has dishes connected in parallel to accommodate a large number of samples. Every branch of the parallel circuit consists of a set of resistors connected in series, R1 to R6 (Fig. 1a): R1-known resistor; R2 = R6-platinum coil immersed in a 20 mL of the electrolyte solution [KCl (0.33 M)] housed in a 25 mL plastic container (polyethylene terephthalate – PET, Kartell); R3 = R5-salt-bridge filled with agar (cell culture tested – A1296, Sigma Aldrich)/KCl (0.33 M) acting as an electrode (Fig. 1b); R4-culture medium ( $\alpha$ -MEM). Advantageously, the conductive electrodes of biological agar depress the toxicological/contamination risks to cells by avoiding the release of oxidative species typically formed at the metallic electrodes and avoids the contamination of other non-metallic electrodes. The extremities of the electrodes (R3 and R5) have a “T” configuration with 5 openings disposed along its length size with a 1 mm diameter and spaced 1 cm apart to ensure a uniform distribution of the electrical fields, and therefore a homogeneous stimulation of the samples. Moreover, the “T” sections of 6 cm in length are smaller than the inner diameter of the culture dish to fit its edge and guarantee the perfect parallelism between the electrodes (I and II, Fig. 1c) resembling capacitive coupled electrodes. The maximum number of 6 samples per culture dish was set after obtaining voltage and current density maps (Fig. 1d and e) of the area between the two electrodes (grey area, Fig. 1c). The maps were obtained under the same conditions used in the stimulation experiments using a reference electrode (A) (Fig. 1c) and equipment described in the experimental section. The area corresponding to the values with the highest uniformity was then selected and used as the stimulation area (delineated with a dotted white line, Fig. 1c–e).

#### 2.5. MG63 osteoblastic-like cell culture

**2.5.1. Cell culture.** Human osteoblastic-like cells (MG63 cells, ATCC number CRL-1427<sup>TM</sup>) were cultured in  $\alpha$ -MEM supplemented with 10% fetal bovine serum, 50  $\mu\text{g mL}^{-1}$  ascorbic acid, 50  $\mu\text{g mL}^{-1}$  gentamicin and 2.5  $\mu\text{g mL}^{-1}$  fungizone at 37 °C in a humidified atmosphere of 5%  $\text{CO}_2$  in air. For sub-culturing, the cell layer (at around 70–80% confluence) was detached with trypsin-EDTA solution (0.05% trypsin, 0.25% EDTA; 5 min, 37 °C). The cell suspension was used in the experiments.

For the cell culture experiments, the material samples were provided as square slices ( $5 \times 5 \times 1 \text{ mm}^3$ ), ground and polished (P4000). Before the *in vitro* testing, the materials were ultrasonically cleaned in ethanol and sterilized using an autoclave.

**2.5.2. Cell culture stimulation.** The waveform and amplitude of the applied electrical stimuli were carefully selected (Table 1) based on three major requisites for bone electrical stimulation: the time-current-voltage response of  $\text{Ca}^{2+}$  ion channels of osteoblastic-like cells to an action potential;<sup>36</sup> the current threshold applied in clinic to efficiently stimulate bone tissue – 5–20  $\mu\text{A}$ ;<sup>9</sup> and the upper limit of current density and electrical field to avoid tissue injury from heat generation – 1–2  $\text{mA cm}^{-2}$  and 10  $\text{V cm}^{-1}$ .<sup>35</sup>

Cells were seeded over standard cell culture coverslips, HA/glass matrix and CNT/HA/glass composite at a density of  $2 \times 10^4$  cells per  $\text{cm}^2$ . Seeded samples, were cultured for 3 days. At this stage, the culture medium was renewed and the colonized samples cultured for further 5 days. During this period, the culture medium was changed twice and the cultures were exposed to a daily electrical stimulation with one of the following conditions: (i) 5  $\mu\text{A}$ , 15 min, (ii) 5  $\mu\text{A}$ , 30 min, (iii) 15  $\mu\text{A}$ , 15 min and (iv) 15  $\mu\text{A}$ , 30 min. Symmetrical biphasic square pulses were used with a fixed frequency and duty cycle value of 40 Hz and 20–80%, respectively, and setting action potential (AP) and resting potential (RP) with fixed periods of 5 and 20 ms, respectively (Fig. 1a). This procedure was repeated daily during the 5 days. Cultures were characterized 24 h after 1, 3 and 5 electrical stimuli. Non-stimulated cultures were run in parallel. Cultures were characterized for DNA content, metabolic activity, and expression of osteoblastic genes, and were observed using scanning electron microscopy (SEM) and confocal laser scanning microscopy (CLSM).

In another experiment, after 3 daily electrical stimuli, the protocol that provided the best stimulation conditions, cultures were maintained for a further 5 days and observed using SEM.

**2.5.3. DNA content.** Non-stimulated and stimulated cultures were evaluated for DNA content using a PicoGreen DNA quantification assay (Quant-iT<sup>TM</sup> PicoGreenR dsDNA Assay Kit, Molecular Probes Inc., Eugene). For that, at each time-point, culture medium was removed and the cultures were treated with Triton X-100 (0.1%) (Sigma) to lyse the cell layer. DNA was assessed in the cellular lysates according to the manufacturer's instructions. Fluorescence was measured on an Elisa reader (Synergy HT, Biotek) at excitation and emission wavelengths of 480 and 520 nm, respectively, and corrected for the fluorescence of the blank reagents. The amount of DNA was calculated by



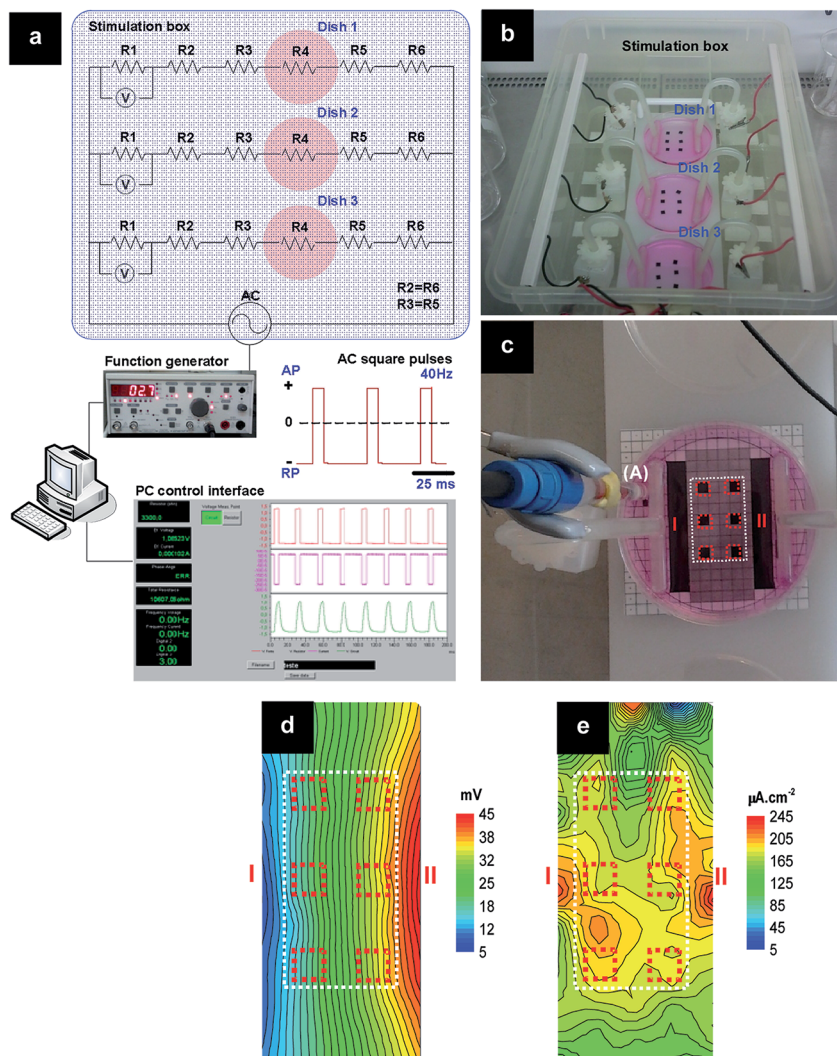


**Fig. 1** (a) A schematic illustration of the electrical stimulation system: stimulation box; function generator, with the respective waveform used (action potentials – AP and resting potentials – RP); and PC control interface. (b) Photographic image of the stimulation box. (c) Magnified photographic image of a culture dish of (b) with parallel disposed salt-bridge electrodes. Color maps of the (d) voltage and (e) current density in the stimulation zone (delineated by a white dotted line).

extrapolating a standard curve obtained by running the assay with the given DNA standard. The results were expressed as a percentage from the control.

**2.5.4. MTT assay.** Metabolic activity of the cell cultures was evaluated using the MTT assay. This is based on the reduction of MTT (3-(4,5-dimethylthiazol-2-yl)-2,5-diphenyltetrazolium) by viable cells to a dark blue formazan product.

At each time-point, MTT ( $0.5 \text{ mg mL}^{-1}$ ) was added to each well and the cultures were incubated for 3 hours at  $37^\circ\text{C}$ . Subsequently, the samples were transferred to new wells and the formazan salts were dissolved in dimethylsulphoxide (DMSO). In addition, a parallel experiment was run with culture medium using the same protocol as the cell cultures, to compensate for the background MTT reduction. The

**Table 1** *In vitro* electrical stimulation metrics of human osteoblastic cells

Stimulation conditions	Resistor, R1 (k $\Omega$ )	Peak-to-peak voltage (V)	Electrical field (mV cm $^{-1}$ )	Current <sub>total</sub> ( $\mu\text{A}$ )	Current <sub>samples</sub> ( $\mu\text{A}$ )	Current density <sub>samples</sub> ( $\mu\text{A cm}^{-2}$ )
5 $\mu\text{A}$ 15 min	3.3	2.7	5.6	100	$5 \pm 2$	$65 \pm 25$
30 min						
15 $\mu\text{A}$ 15 min	1.5	4	15.3	200	$15 \pm 3$	$185 \pm 30$
30 min						



optical density (OD) was determined at  $\lambda = 600$  nm on an Elisa reader (Synergy HT, Biotek). The results were expressed as a percentage from the control.

**2.5.5. Gene expression.** Cultures were assessed by RT-PCR after 5 daily stimuli for the expression of the housekeeping gene glycerol-3-phosphate dehydrogenase (GAPDH), the transcription factor Runx2 and the osteoblastic genes collagen type I (Col I), alkaline phosphatase (ALP), osteocalcin (OC) and osteoprotegerin (OPG). For that, RNA was extracted using a Rneasy® Mini Kit (QIAGEN) according to the manufacturer's instructions and quantified using UV spectrophotometry at 260 nm. Half microgram of RNA was reverse transcribed and amplified (25 cycles) with the Titan One Tube RT-PCR System (Roche) with an annealing temperature of 55 °C. Table 2 shows the primers used in the RT-PCR analysis. After electrophoresis on 1% (w/v) agarose gel, the bands were analysed by densitometry with ImageJ 1.41 software. Values were normalized to the corresponding GAPDH value of each experimental condition.

**2.5.6. SEM and CLSM observation.** For SEM observation, samples were fixed (1.5% glutaraldehyde in 0.14 M sodium cacodylate buffer, pH = 7.3, 10 min), dehydrated in graded alcohols, critical-point dried, sputter-coated with an Au/Pd thin film (SPI Module Sputter Coater equipment) and observed under a high resolution (Schottky) environmental scanning electron microscope (Quanta 400 FEG ESEM). For confocal laser scanning microscopy (CLSM) assessment, samples were fixed (3.7% paraformaldehyde, 15 min). Cell cytoskeleton filamentous actin (F-actin) was visualized by treating the cells with Alexa Fluor 488 Phalloidin (1 : 20 dilution in PBS, 1 h) and counterstaining with propidium iodide (1  $\mu\text{g mL}^{-1}$ , 10 min) for cell nuclei labelling. The labelled cultures were mounted in Vectashield® and examined under a Leica SP2 AOBs (Leica Microsystems) microscope.

**2.5.7. Statistical analysis.** Three independent experiments were performed; in each experiment, three replicas were accomplished for the biochemical assays and two replicas for the qualitative assays. The results are presented as the mean  $\pm$  standard deviation (SD). Groups of data were evaluated using a two-way analysis of variance (ANOVA) and no significant differences in the pattern of the cell behavior found. Statistical differences between experimental groups were assessed by Bonferroni's method. Values of  $p \leq 0.05$  were considered as statistically significant.

### 3. Results and discussion

#### 3.1. Microstructural and mechanical characterization of the bone grafts

Bone grafts are expected to restore the skeletal integrity by offering biological functional and mechanical supports during bone repairing. To ensure these functionalities, bone grafts scaffolds should fulfill the following main requisites:<sup>2</sup> (1) biodegradable with non-cytotoxic degradation by-products; and (2) mechanical properties close to those of bone, to maintain its structural integrity, and therefore preserve the porous network during the first stages of new bone formation. To match this biological profile, it becomes mandatory to control the CNT agglomeration state in the consolidated bioceramic composites. In this respect, a thorough characterization of the microstructure and mechanical properties of the materials are reported in the present section.

For the preparation of the composite materials, under a hot-pressing temperature of 1100 °C the glass reacts with the hydroxyapatite causing its partly conversion into the  $\beta$ -TCP (tricalcium phosphate) phase, as depicted in the X-ray diffraction patterns shown in Fig. 2a and b for the HA/glass matrix and the 4.4 vol% CNT/HA/glass composite, respectively. The peaks correspond to those reported in the Joint Committee on Powder Diffraction Standards (JCPDS) files for HA (JCPDS 72-1243) and  $\beta$ -tricalcium phosphate,  $\beta$ -TCP (JCPDS 09-0169). By comparing these two plots, it becomes quite clear that there are almost no changes in the phase composition when the CNTs are added to the matrix. Arquimedes' density showed that the HA/glass matrix is almost fully dense. The scanning electron microscopy (SEM) micrographs of the polished surfaces of the unreinforced matrix and the 4.4 vol% CNT composite after immersion in  $\alpha$ -MEM in Fig. 2c and d show some well distributed porosity as a result of preferential leaching of the  $\beta$ -TCP phase.<sup>37</sup> This effect is further enhanced in the presence of CNTs, as is clear from the observation of the microstructure of the 4.4 vol% CNT composite shown in Fig. 2d. The material surrounding the pore-like defects due to  $\alpha$ -MEM preferential attack is less dense with evidence of microporosity that is not present in the HA/glass matrix. Moreover, from the SEM observations there are no clearly identifiable zones containing individualized CNTs.

The use of Raman spectroscopy in imaging mode permitted the areas in the dense materials in which HA,  $\beta$ -TCP and CNTs were present to be clearly identified, as shown in Fig. 2e and f.<sup>38</sup> The image of the unreinforced matrix (Fig. 2e) and the spectra

Table 2 Primers used on RT-PCR analysis

Gene	Forward primer	Reverse primer
GAPDH	CAGGACCAGGTTACCAACAAGT	GTGGCAGTGATGGCATGGACTGT
Runx2	CAGTTCCCAAGCATTTTCATCC	TCAATATGGTCGCCAAACAG
COL1	TCCGGCTCCTGCTCCTCTTA	ACCAGCAGGACCAGCATCTC
ALP	ACGTGGCTAAGAATGTCATC	CTGGTAGGCGATGTCCTTA
OC	CACTCCTCGCCCTATTG	CCCACAGATTCTCTTCT
OPG	AAGGAGCTGCAGTAGGTCAA	CTGCTCGAAGGTGAGGTTAG

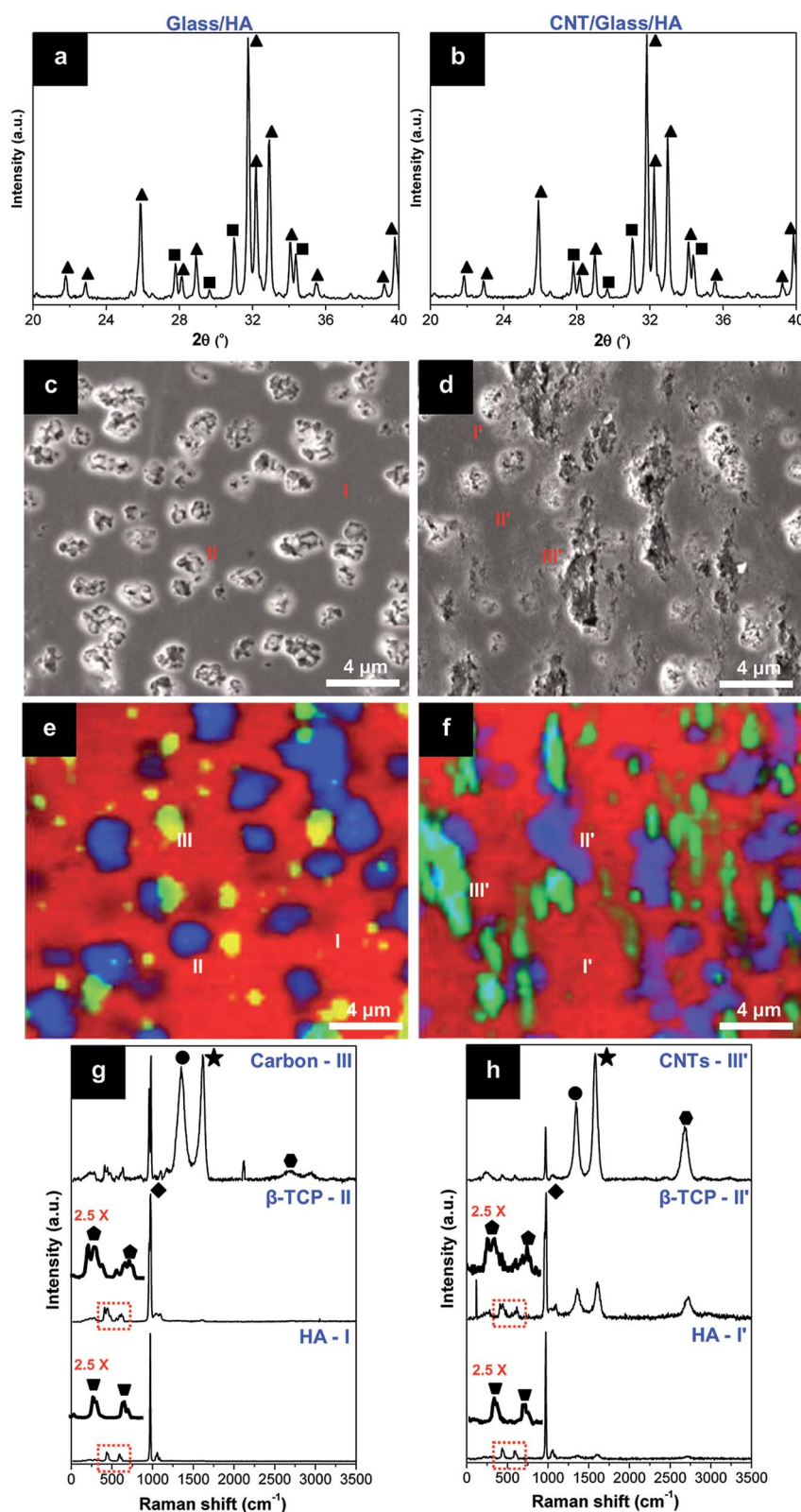


Fig. 2 XRD spectra of hot-pressed (a) glass/HA and (b) CNT/glass/HA compacts. (■)  $\beta$ -TCP, (▲) HA (c and d) SEM micrographs of (a) and (b). (e and f) Colour Raman maps and respective (g and h) spectra of (a) and (b) (carbon and CNTs: ●: D-band, ★: G-band, ●: G'(2D)-band;  $\beta$ -TCP: ◆:  $\nu_1$ - $\text{PO}_3^{2-}$ , ▼:  $\nu_2$ - $\text{PO}_3^{2-}$ ; HA: ◆:  $\nu_1$ - $\text{PO}_3^{2-}$ , ▼:  $\nu_2$ - $\text{PO}_3^{2-}$ ).

in Fig. 2g help to show that the pore-like defects were associated to the  $\beta$ -TCP phase location. Furthermore, there is carbon contamination during the hot-pressing process using graphite dies at temperatures where the HA/glass matrix is quite chemically active. This contamination is not so clear in the Raman mapping for the 4.4 vol% CNT composite, as shown in Fig. 2f. By combining the code colors shown in Fig. 2f with the corresponding spectra (Fig. 2h), it becomes clear that CNTs (addressed by the  $G'$  (2D) signature and higher G/D ratio) are present mainly as elongated agglomerates but can be identified throughout the matrix within the resolution limits of the technique. It is worth noting that the observed SEM surfaces are parallel to the pressing direction and this accounts for the pressure induced alignment observed for the large agglomerates of CNTs in the 4.4 vol% CNT material (Fig. 2d). The 6% porosity measured in this material by Arquimedes' immersion reflects not only the damping effect of the CNTs and the difficulty in transmitting the pressure to the HA/glass matrix for densification, but also the increased interactions and entanglement of the CNT agglomerates that further prevent matrix contiguity from happening. This porosity is closer to the cortical bone than the glass/HA matrix alone, that is almost fully dense but still reacts readily with  $\alpha$ -MEM, as shown in Fig. 2c. Nevertheless, both the compressive and bending strength of the produced materials have values that are well within or above cortical bone specifications for adult, healthy individuals with average values of compressive and bending strengths of 700 MPa and 160 MPa, respectively, for the 4.4 vol% CNT/HA/glass composite.

### 3.2. Bone grafts- $\alpha$ -MEM culture medium interactions

A key idea of the present work is to make the electrical stimulus converge through the osteoblasts present at the composite surface in order to tune its cellular functions. Fig. 3a gives the conductivity of the culture medium  $\alpha$ -MEM and several biological tissues/organs/milieus together with the new CNT/glass/HA material (labeled as blue).<sup>39</sup> It can be seen that the CNT composite has a higher conductivity than the *in vitro* culture medium or any other *in vivo* environment. In line with this, it is expected that this characteristic yield CNTs containing substrates with high potential to increase the local conductivity and confine electrical fields, making them highly efficient electron conductors and delivering pathway systems.

To ensure the validity of this hypothesis and the experimental approach used for cell stimulation, a set of preliminary studies were carried out: (1) by studying the effects on the resistivity of  $\alpha$ -MEM using immersed conducting and non-conducting samples; and (2) by identifying the current density (electric field) lines on samples of different geometries.

**3.2.1. Neutral conditions.** The electrochemical cells contained  $\alpha$ -MEM and 6 or 12 samples (example in Fig. 3b). The impedance of the cell was measured in a two electrode arrangement using 2 platinum spiral electrodes. The variation of the modulus of impedance,  $|Z|$ , with the signal frequency is shown in Fig. 3c. The values were normalized to the area of the electrodes. The impedance response shows two regions, one at

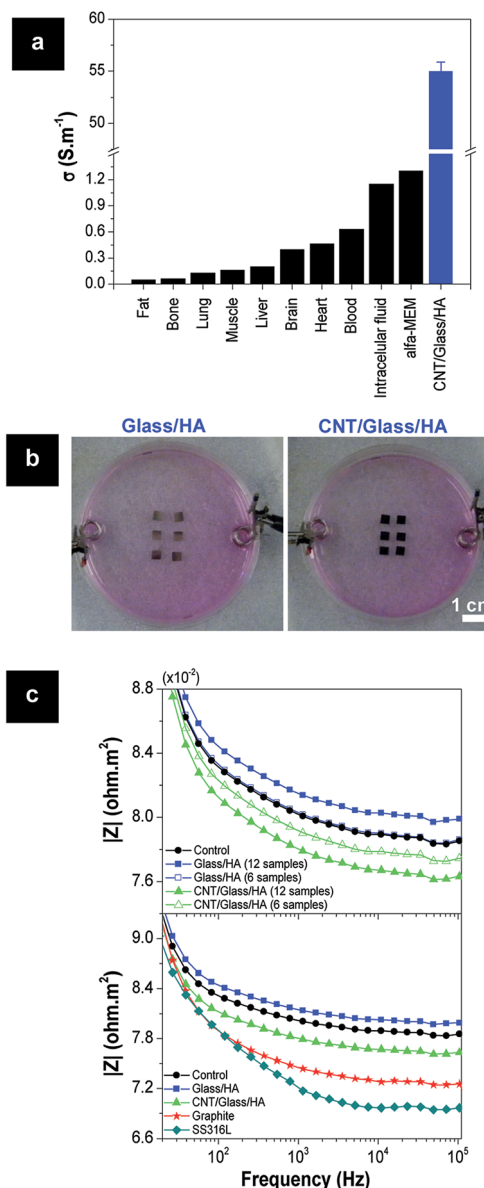


Fig. 3 (a) A plot comparing the electrical conductivity of biological tissues and milieus,<sup>39</sup>  $\alpha$ -MEM and the CNT/glass/HA composite (highlighted in blue). (b) Photographs of the electrochemical cells with 6 samples immersed in 12 mL of  $\alpha$ -MEM and the platinum spiral electrodes. (c) Plots showing the dependence of the modulus of impedance  $|Z|$  of the electrochemical cells on the signal frequency.

higher frequencies with constant  $|Z|$  and another at frequencies below  $\sim 5$  kHz where  $|Z|$  increases as the frequency decreases. The high frequency region is related to the solution resistance, while the second one measures the double layer capacitance at the surface of the Pt electrodes. Thus, only the high frequency part is of interest to this study.

The control curve is simply the resistance of  $\alpha$ -MEM. The other curves show the resistance when 6 or 12 samples of either glass/HA (non-conductive) or CNT/glass/HA (conductive) were immersed in solution. The resistance increased with 12 non-conductive samples and decreased with a decrease proportional to the number of pieces when conductive pieces were used. The



same experiment with different materials showed that the more conductive the material is the lower the resistance of the medium.

**3.2.2. Electrical stimulation conditions.** The current lines in solution near the conductive samples when placed in an electrochemical cell were measured using a vibrating voltage probe. Fig. 4a depicts the experimental set up with a fixed current running from one electrode plate to the other, both disposed in parallel. Part of the current flows through the sample and the remaining current will diverge, surrounding the sample because it represents an obstacle to flow. A component of the current normal to the surface could be detected, having a positive sign on the side of the positive electrode because the current lines move up and negative on the right because the

current lines descend, returning to their original path in the solution as can be seen in Fig. 4b. The closer the line of measurement is to the sample, the higher is the measured normal component. A distance of 50  $\mu\text{m}$  provided the highest sensitivity to the normal current whilst avoiding the risk of the probe touching the sample. The experiment was repeated with different materials, as shown in Fig. 4c. The decrease in the normal component for higher conductive materials proves that the current is converging through the material to a higher extent for the more conductive materials (steel and graphite).

The influence of the sample geometry on current distribution was also investigated because CNT/glass/HA bone grafts may be applied as granules having irregular shapes. It is therefore important to check if geometry is a factor to be

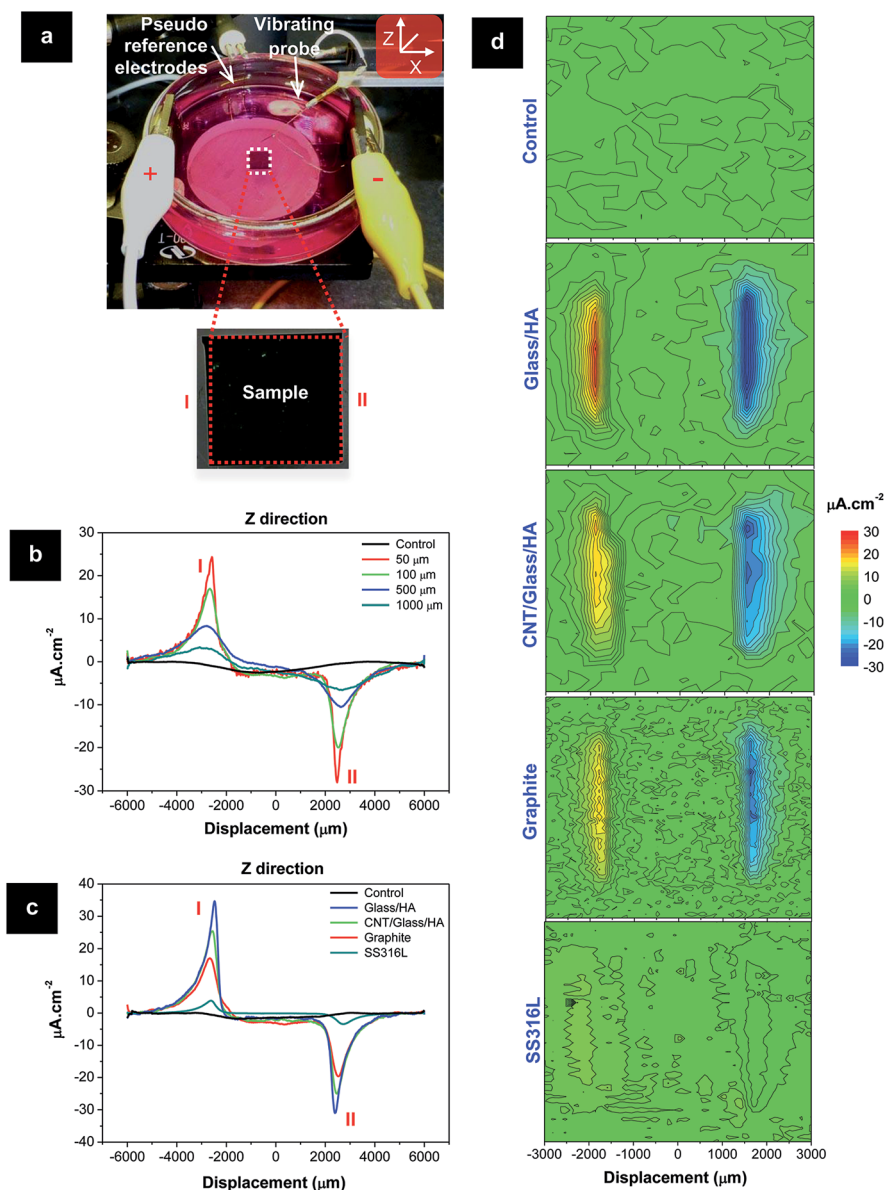


Fig. 4 (a) Set-up of the vibrating voltage probe measuring system in an electrochemical cell containing parallel graphite electrodes and one sample at the centre immersed in 12 ml of  $\alpha$ -MEM. (b) Plot of the variation of current density in the z direction following lines from I to II (see sample scheme in a) at different heights from the sample. (c) Plot of the variation of current density in the z direction 50  $\mu\text{m}$  above samples of materials with different electrical conductivity. (d) Same as (c) but with maps in a plane parallel to the samples.

considered in the electrical field distribution. The results in Fig. 5 show that no significant differences in the  $z$  component of current density,  $I_z$ , exist for triangular, round and rectangular shaped samples. Moreover, the correspondent  $I_z$  values for CNT/glass/HA and glass/HA samples are still close to one another and have lower values, corroborating data of Fig. 5b.

### 3.3. Osteoblastic cells proliferation and gene expression: substrate efficiency in the delivery of stimulus *in situ*

The MG63 cell line was used to address the potential role of the electroconductivity of the CNT/HA/glass composite on the osteoblastic cell response under electrical stimulation and to select an optimized set of conditions for improved cell behaviour. This cell system provides a homogeneous, phenotypically stable and proliferative population that shows many phenotypic features of normal osteoblastic cells, including hormonal responsiveness and expression of early and late stage osteogenic genes, being widely used as a osteoblast cell model for *in vitro* research.<sup>40</sup> Cell cultures, performed on standard cell culture coverslips, HA/glass matrix and CNT/HA/glass composite were submitted to electrical stimuli of 5  $\mu$ A/15 min, 5  $\mu$ A/30 min, 15  $\mu$ A/15 min or 15  $\mu$ A/30 min (Table 1), one time a day for five consecutive days, and were assessed 24 h after 1, 3

and 5 stimuli for the DNA content, metabolic activity and gene expression of Runx2 (Runt-related transcription factor 2), Col I (Collagen type I), ALP (Alkaline Phosphatase), OC (Osteocalcin) and OPG (Osteoprotegerin).

The DNA content on the cultured coverslip and on the two materials, in non-stimulated conditions, increased throughout the culture time. This parameter reflects the number of cells present on the substrates being an index of the cell proliferation. Under electrical stimulation, the DNA content on the CNT/HA/glass composite was greatly increased after 1 and 3 stimuli ( $\sim 25\%$  to  $60\%$ ) and was similar after 5 days of treatments when compared to the non-stimulated cultures (Fig. 6c). The inductive effect was dependent on the stimulus intensity and duration, and was higher with 15  $\mu$ A, 30 min (after 1 stimulus,  $\sim 60\%$ ) and 15  $\mu$ A, 15 min (after 3 stimuli,  $\sim 62\%$ ). Cell response over the dielectric surfaces (coverslip and HA/glass matrix) was similar under electrical stimulation (Fig. 6a and b). When compared to non-stimulated cultures, the DNA content was slightly increased, similar and significantly lower after 1, 3 and 5 daily treatments.

The results for the MTT reduction (Fig. 6d–f), a metabolic activity/proliferation assay based on the reduction ability of cell mitochondrial dehydrogenases showed a pattern similar to that observed for the DNA content, in the conductive and dielectric

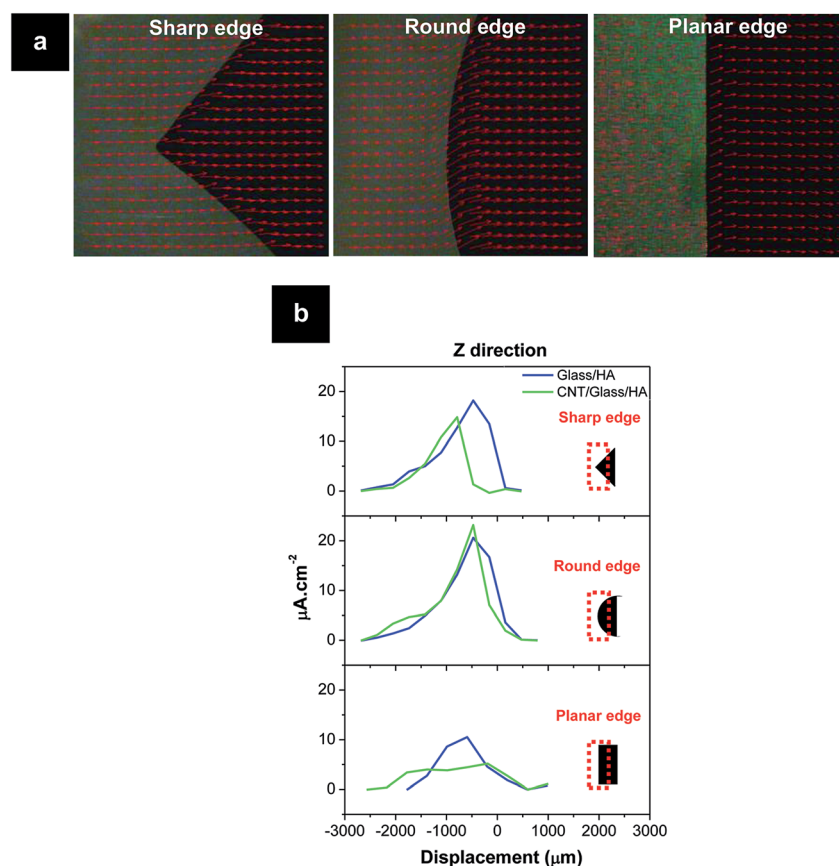


Fig. 5 (a) Photographs showing the 2D distribution of the current density vectors ( $I_x$ ,  $I_z$ ) for CNT/Glass/HA samples with different edge geometries. (b) Plots of the variation of the current density in the  $z$  direction in lines 50  $\mu$ m above samples of Glass/HA and CNT/Glass/HA with different edge geometry.

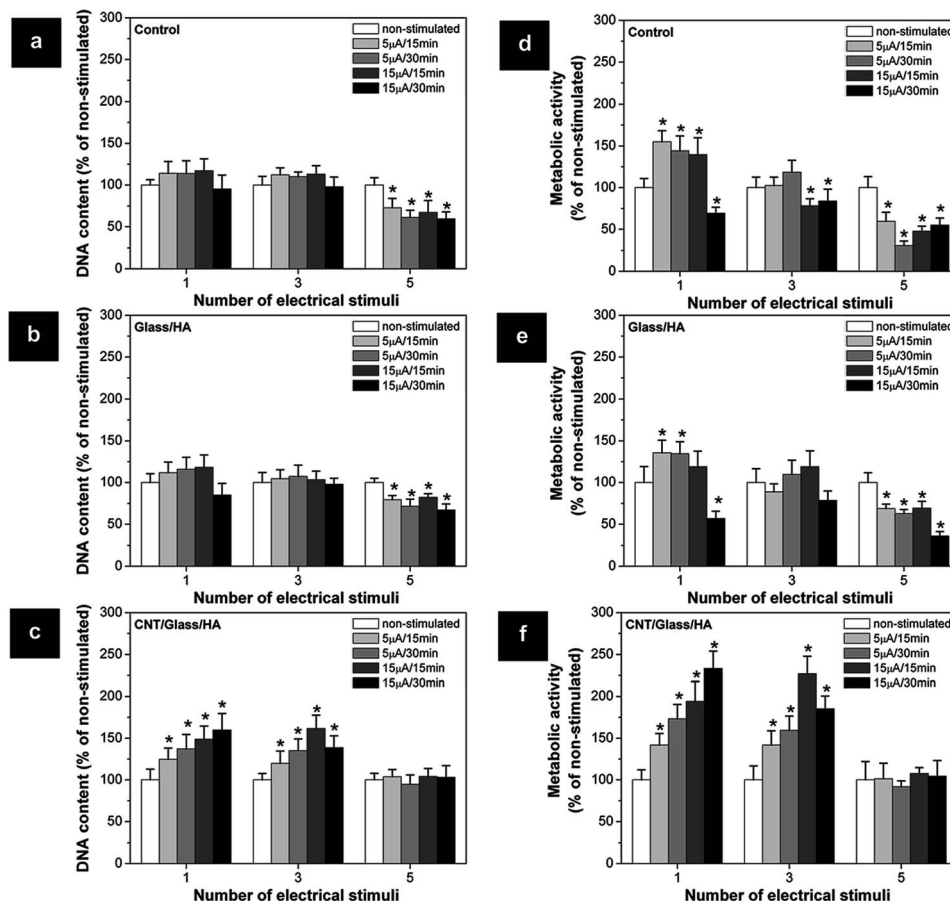


Fig. 6 (a–c) DNA content and (d–f) cell viability/proliferation of osteoblastic cell cultures grown over standard cell culture coverslips, glass/HA matrix and the CNT/glass/HA composite characterized 24 h after 1, 3, and 5 daily electrical stimuli, under different stimulation conditions. The results are expressed as a percentage of variation from the non-stimulated cultures. \* Significantly different from the non-stimulated cultures.

substrates. However, in both types of surfaces, for the inductive effects, the percentage increase in the OD values reflecting the metabolic activity was always higher than that found for the DNA content. Therefore, for the CNT/HA/glass composite, increases of ~40% to 130% were found after 1 and 3 stimuli. Hence, under selected stimulation conditions, both the cell proliferation and the metabolic activity were induced suggesting the presence of a higher number of cells with increased metabolic activity compared to the non-stimulated conditions. However, these cellular parameters decreased following repeated stimuli. This behaviour has been previously reported and appears to be conditioned by the stage of cell differentiation.<sup>41,42</sup>

Cultures were characterized for mRNA expression of several osteoblastic genes, 24 h after 5 daily electrical stimuli under (15  $\mu$ A, 15 min) (Fig. 7). The results show that the expression of Runx2 was particularly sensitive to the inductive effects of electrical stimulation. It was up-regulated on cultures grown over the CNT/HA/glass composite, and also on those over the HA/glass matrix. Even in the cultured coverslip, which showed a low expression of Runx2 in the non-stimulated cultures, there was a trend for an increase under stimulated conditions. This is

an interesting finding, as Runx2 is the earliest transcription factor for osteogenic differentiation and, in addition, it activates the expression of multiple late stage osteoblastic genes.<sup>35</sup> Over the stimulated CNT/HA/glass composite, there was also increased mRNA expression for ALP and OC an early and a late stage marker in the osteogenic differentiation pathway, respectively. As both molecules have a role in the extracellular matrix mineralization in the initiation of mineral deposition (ALP) and the regulation of crystal growth (OC),<sup>43</sup> this observation points to an enhanced osteogenic differentiation under electrical stimulation. No effect was noted on the expression of Col 1 and OPG. Col 1 is the most abundant extracellular bone matrix, considered an early bone differentiation marker, which has a role in osteoblastic differentiation and also in the nucleation site and growth space of hydroxyapatite.<sup>44,45</sup> On the other hand, OPG is a key molecule in the interplay between osteoblasts and osteoclasts during bone remodelling. It is a decoy receptor that binds to RANKL, blocking its binding to the RANK receptor on osteoclasts, which inhibits osteoclastogenesis.<sup>46</sup> These results on the gene expression might suggest that electrical stimulation induces the osteogenic differentiation and, eventually, may also enhance the level of matrix mineralization



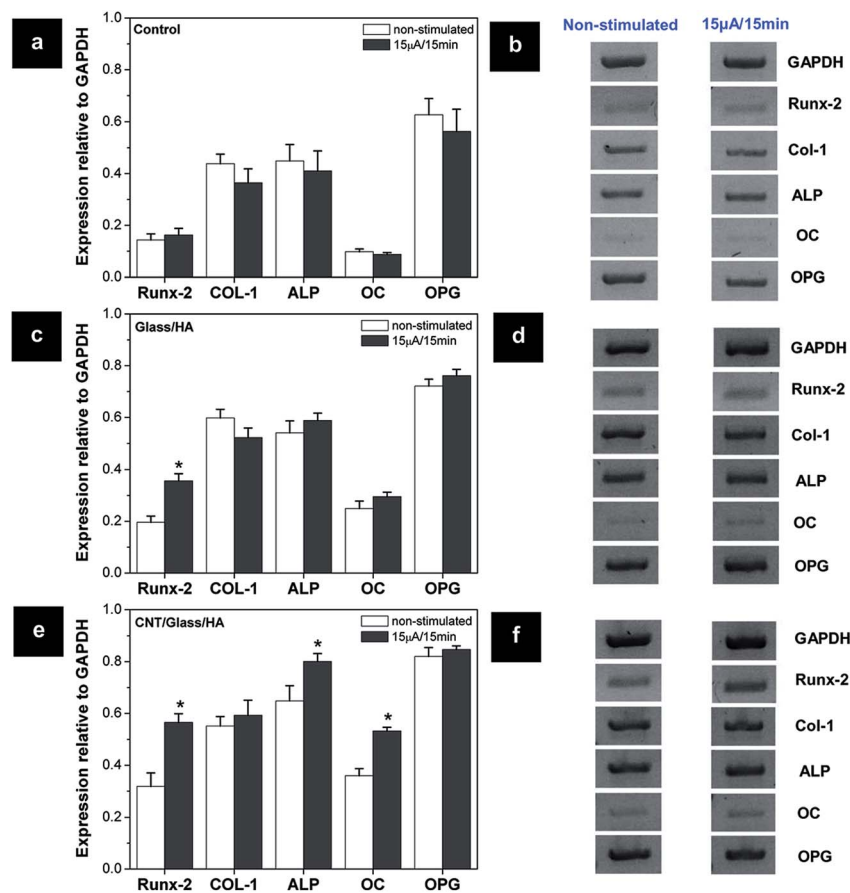


Fig. 7 Expression of osteoblastic-related genes by cell cultures grown over standard cell culture coverslips, glass/HA matrix and the CNT/glass/HA composite characterized 24 h after 5 daily electrical stimuli (15  $\mu$ A, 15 min). The results are expressed as a percentage of variation from the non-stimulated cultures. Densitometric analysis of the RT-PCR bands normalized to the corresponding GAPDH value (a, c, e) and representative images of the PCR products in the agarose gel (b, d, f). \* Significantly different from the non-stimulated cultures.

of the collagenous extracellular matrix. Additionally, the osteoblast/osteoclast interactions regarding the modulation of osteoclastogenesis *via* OPG appear not to be affected. Overall, such a profile would be interesting to speed up the initial material stabilization leading to a faster osteointegration process.

On CLSM (Fig. 8), non-stimulated and stimulated cells (observed 24 h after 1 and 3 daily electrical stimuli, 15  $\mu$ A/15 min) displayed a polygonal/elongated morphology on the HA/glass matrix and, essentially, an elongated/fusiform appearance on the CNT/HA/glass composite. On both the surfaces, cells exhibited a well-organized F-actin cytoskeleton, with intense staining at the cell boundaries, prominent nucleus and ongoing cell division, signs of mechanical integrity and healthy behaviour. Over the CNT/HA/glass composite, a specific cell orientation was already visible at day 1 and a characteristic aligned cell growth was evident at later culture times, when compared to the random pattern of cell growth seen over the HA/glass matrix. SEM observation of the same cultures (Fig. 9a) provided similar information but, additionally, the images showed that the organization of the cell layer over the CNT/HA/glass composite followed the alignment direction of the CNT agglomerates on the glass/HA matrix. This behaviour was

evident since the beginning of the culture time, as seen 24 h after 1 electrical stimulus, and also over longer culture times, *i.e.* 24 h after 3 electrical stimuli. The cultures were also observed 5 days after 3 daily electrical stimuli (15  $\mu$ A/15 min). The SEM images showed an abundant and well-organized cell layer over the three surfaces, which showed that cell proliferation increased with the culture time. Moreover, cells presented a healthy morphology and intimate cell-to-cell contact. Representative images of the stimulated cultures are shown in Fig. 9b and it is noteworthy that the cultures grown over the CNT/glass/HA composites still maintained a well-defined alignment. Additionally, a high magnification SEM image showed a close interaction between the surface of a well spread cell and the CNT network on the composite structure.

This observation is in line with some reported information, showing that aligned CNT networks exhibited the ability to modulate cell morphology and the directional growth of human osteoblastic cells, in comparison to the seeded and randomly oriented CNT network.<sup>47,48</sup> In general, the electrical stimulation did not result in evident effects in the aligned cell organization over the CNT/HA/glass composite. The distinct cytoskeleton organization over the CNT/HA/glass and HA/glass samples was expected to modulate the cell response to the two substrates.

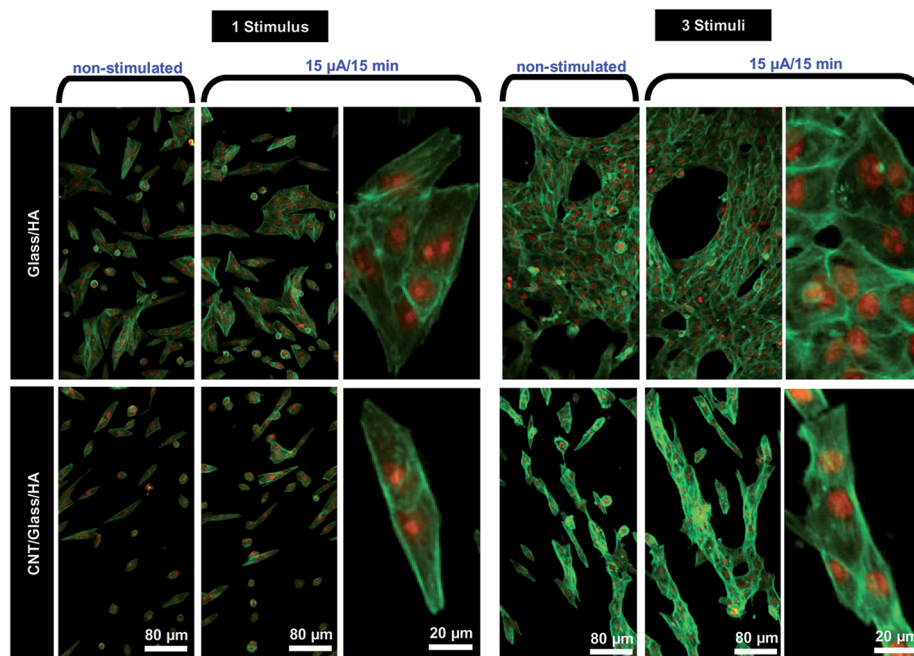


Fig. 8 CLSM appearance of osteoblastic cell cultures grown over the glass/HA matrix and CNT/glass/HA composite observed 24 h after 1 and 3 daily electrical stimuli under different stimulation conditions. The cells were stained for the F-actin cytoskeleton (green) and nucleus (red).

The F-actin cytoskeleton, which is highly concentrated just beneath the plasma membrane, provides structural stability and elasticity to the cell undergoing substrate adaptation, but it is also a key player in the cellular mechano-transduction mechanisms modulating complex signalling pathways such as the Rho family GTPases, which affect the overall cell behaviour.<sup>49</sup> Related to this, it has been suggested that the directional cell growth observed in aligned CNTs structures enhances osteogenic differentiation, in comparison to the seeded and randomly oriented CNTs network, a process possibly mediated by the high cytoskeleton tension accumulated on aligned cells leading to the activation of selective mechano-transduction pathways.<sup>48</sup>

The results show that under an appropriate electrical stimulation protocol, the conductive CNT/HA/glass composite exhibited significantly improved cell proliferation, metabolic activity and osteoblastic gene expression. The lower inductive effect on cell proliferation but higher expression of relevant osteogenic genes and ALP activity found over the CNT/HA/glass composite after few stimuli suggest an inductive effect on the osteoblastic differentiation, taking into account the established reciprocal relationship between proliferation and differentiation during the development of the osteoblastic phenotype.<sup>44</sup>

Briefly, cell function activity was significantly improved on the CNT/HA/glass composite, which is intimately related with its efficiency in the delivery of electrical stimuli to cells. According to Section 3.2, conductive substrates increase the local conductivity of the culture medium and render the confinement of the exogenous electrical fields on the surface of the material. Fig. 10 sketches the interaction of the electrical field lines with cells surrounding non-conductive and conductive substrates. In the latter, the electrical field confinement

(higher current density) at perpendicular angles to the surface<sup>39</sup> imposes osteoblastic cells in contact to be crossed by the electrical fields. Contrarily, in a dielectric material the external fields are parallel to its surface, and are not confined, and therefore a considerably lower efficiency of stimuli delivery at the sample surface is observed relative to the conductor material.

Regarding the mechanisms involved, electrical stimulation seems to modulate cell behaviour essentially by altering the intracellular calcium dynamics.<sup>49</sup> Although being a versatile process and likely to depend on the cell type and microenvironmental conditions, the modulation of the intracellular calcium levels in human mesenchymal stem cells seems to be involved in directing their osteogenic differentiation.<sup>49–51</sup> Associated mechanisms appear to be related with the clustering and activation of cell-surface receptors (*e.g.* integrins), interaction with G-protein coupled receptors (*e.g.* PLC – phospholipase C), ATP (adenosine 5'-triphosphate) release and activation of ion channels. Regarding the latter, the intracellular calcium can be raised inside osteoblastic cells by  $\text{Ca}^{2+}$  transport *via* L-type  $\text{Ca}^{2+}$  channels.<sup>52,53</sup> Of interest, it was found that these ion channels preferentially regulate  $\text{Ca}^{2+}$ -dependent genes and enzymes, such as the  $\text{Ca}^{2+}$ /calmodulin-dependent protein kinase II (CaMKII),<sup>54</sup> a key pathway towards the regulation of osteoblast proliferation/differentiation.<sup>55</sup> In the present work, the high current-voltage thresholds of osteoblastic  $\text{Ca}^{2+}$  ion channels gives further evidence that cell response to stimuli appears to be L-type  $\text{Ca}^{2+}$ /CaMKII mediated because cell proliferation and metabolic activity were maximized for the high current stimuli conditions (15  $\mu\text{A}$ , 15 min). Moreover, when compared to glass/HA, the conductive CNT/glass/HA composite reveals a higher activation of L-type ion channels (*i.e.* intracellular  $\text{Ca}^{2+}$  levels)

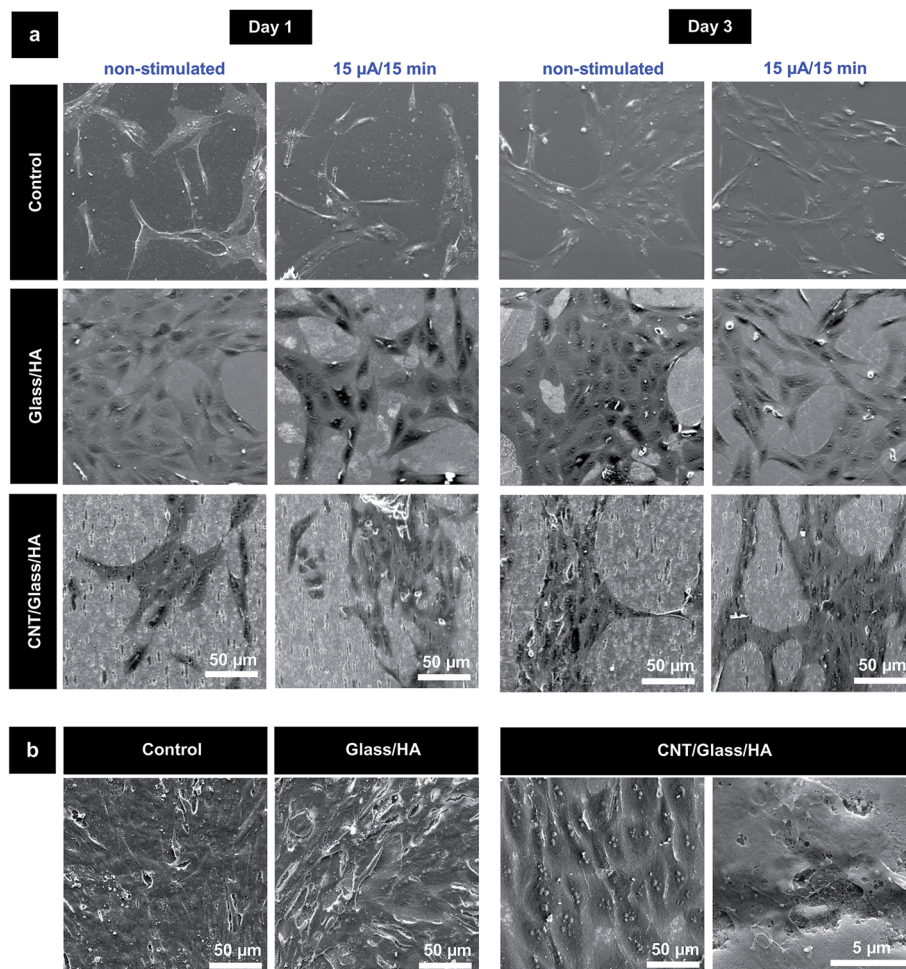


Fig. 9 (a) SEM appearance of osteoblastic cell cultures grown over standard cell culture cover slips, glass/HA composite and the CNT/glass/HA composite observed 24 h after 1 and 3 daily electrical stimuli ( $15 \mu\text{A}/15 \text{ min}$ ). (b) SEM appearance of the cultures observed 5 days after the 3 daily electrical stimuli ( $15 \mu\text{A}/15 \text{ min}$ ); the panel also displays a high magnification image of the CNT/glass/HA composite showing a close interaction between the osteoblastic cells and the CNT on the composite matrix.

and larger efficiency of bone cell stimulation. This may be related to the high efficiency of charge transfer voltage at the substrate–cell interface related to the high density of electric

field lines crossing the cell (Fig. 10), which boosts the opening of voltage-gated channels at multi-locations in the cell membrane and raises the magnitude of the action potential.

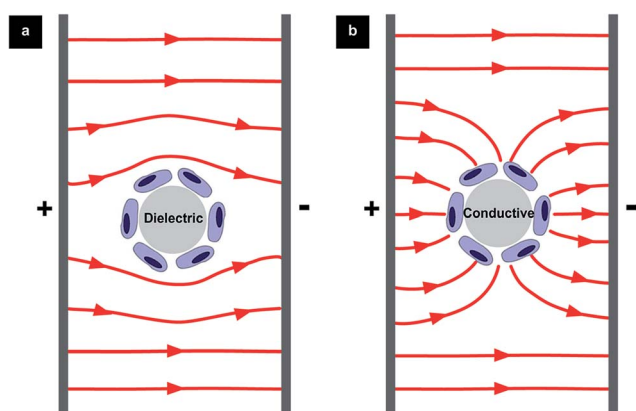


Fig. 10 Top view schematic images of the electric field (current density) lines distribution of (a) dielectric and (b) conductive spherical samples interfacing with osteoblastic cells (elliptical purple sketches) immersed in a homogeneous  $\alpha$ -MEM culture medium.

## 4. Conclusions

In the present study, the conductive CNT/HA/glass composite showed significantly improved cell functional activity under an appropriate electrical stimulation protocol when compared to the HA/glass matrix. The cell metabolic activity and DNA content were increased by 130% and 60%, relatively to the non-stimulated conditions, after only 3 days of daily stimulation of  $15 \mu\text{A}$  for 15 min. Moreover, the osteoblastic gene expression for Runx2, OC and ALP was enhanced by 80%, 50% and 25%, respectively, after 5 days of stimulation. These observations were closely related to the local increase in the culture medium conductivity and the confinement of electrical fields on the surface of the conductive material. This experimental evidence of selective bone cell stimulation on conductive bone grafts will offer new possibilities in non-invasive clinic electrotherapies.



## Acknowledgements

D. Mata acknowledges Foundation for Science and Technology (FCT, Portugal) for funding the project PEst-C/CTM/LA0011/2013. M. Belmonte acknowledges the financial support of the Spanish Government (project MAT2012-32944).

## References

- 1 M. M. Stevens, *Mater. Today*, 2008, **11**, 18–25.
- 2 M. Navarro, A. Michiardi, O. Castaño and J. A. Planell, *J. R. Soc., Interface*, 2008, **5**, 1137–1158.
- 3 R. Spear and R. Cameron, *International Journal of Material Forming*, 2008, **1**, 127–133.
- 4 C. A. L. Bassett and R. O. Becker, *Science*, 1962, **137**, 1063–1064.
- 5 E. Fukada and I. Yasuda, *J. Phys. Soc. Jpn.*, 1957, **12**, 1158–1162.
- 6 C. Bassett, *CRC Crit. Rev. Bioeng.*, 1989, **17**, 451–529.
- 7 M. Zayzafoon, *J. Cell. Biochem.*, 2006, **97**, 56–70.
- 8 F. Bezanilla, *Physiol. Rev.*, 2000, **80**, 555–592.
- 9 M. Griffin and A. Bayat, *ePlasty*, 2011, **11**, 303–353.
- 10 M. Griffin, S. Iqbal, A. Sebastian, J. Colthurst and A. Bayat, *J. Bone Jt. Surg., Br. Vol.*, 2012, **94**, 33.
- 11 D. G. Woo, M.-S. Shim, J. S. Park, H. N. Yang, D.-R. Lee and K.-H. Park, *Biomaterials*, 2009, **30**, 5631–5638.
- 12 Z. Schwartz, B. J. Simon, M. A. Duran, G. Barabino, R. Chaudhri and B. D. Boyan, *J. Orthop. Res.*, 2008, **26**, 1250–1255.
- 13 M. Akai and K. Hayashi, *Bioelectromagnetics*, 2002, **23**, 132–143.
- 14 W. M. Novicoff, A. Manaswi, M. V. Hogan, S. M. Brubaker, W. M. Mihalko and K. J. Saleh, *Critical Analysis of the Evidence for Current Technologies in Bone-Healing and Repair*, 2008, vol. 90, pp. 85–91.
- 15 S. B. Behrens, M. E. Deren and K. O. Monchik, *Curr. Orthop. Pract.*, 2013, **24**, 84–91.
- 16 P. R. Supronowicz, P. M. Ajayan, K. R. Ullmann, B. P. Arulanandam, D. W. Metzger and R. Bizios, *J. Biomed. Mater. Res.*, 2002, **59**, 499–506.
- 17 S. Meng, M. Rouabhi and Z. Zhang, *Bioelectromagnetics*, 2013, **34**, 189–199.
- 18 S. Orrenius, B. Zhivotovsky and P. Nicotera, *Nat. Rev. Mol. Cell Biol.*, 2003, **4**, 552–565.
- 19 G. Ermak and K. J. A. Davies, *Mol. Immunol.*, 2002, **38**, 713–721.
- 20 D. A. Puleo and W. W. Huh, *J. Appl. Biomater.*, 1995, **6**, 109–116.
- 21 J. Zhang, K. G. Neoh, X. Hu, E.-T. Kang and W. Wang, *Biotechnol. Bioeng.*, 2013, **110**, 1466–1475.
- 22 K. Sahithi, M. Swetha, K. Ramasamy, N. Srinivasan and N. Selvamurugan, *Int. J. Biol. Macromol.*, 2010, **46**, 281–283.
- 23 M. Vila, M. Cicuéndez, J. Sánchez-Marcos, V. Fal-Miyar, M. Manzano, C. Prieto and M. Vallet-Regi, *J. Biomed. Mater. Res., Part A*, 2013, **101**, 213–221.
- 24 S. Facca, D. Lahiri, F. Fioretti, N. Messadeq, D. Mainard, N. Benkirane-Jessel and A. Agarwal, *ACS Nano*, 2011, **5**, 4790–4799.
- 25 D. Lahiri, V. Singh, A. K. Keshri, S. Seal and A. Agarwal, *Carbon*, 2010, **48**, 3103–3120.
- 26 C. A. Poland, R. Duffin, I. Kinloch, A. Maynard, W. A. Wallace, A. Seaton, V. Stone, S. Brown, W. MacNee and K. Donaldson, *Nat. Nanotechnol.*, 2008, **3**, 423–428.
- 27 J. Meng, L. Song, H. Kong, G. Zhu, C. Wang, L. Xu, S. Xie and H. Xu, *J. Biomed. Mater. Res., Part A*, 2006, **79**, 298–306.
- 28 M. A. Correa-Duarte, N. Wagner, J. Rojas-Chapana, C. Morszeck, M. Thie and M. Giersig, *Nano Lett.*, 2004, **4**, 2233–2236.
- 29 D. A. LaVan, T. McGuire and R. Langer, *Nat. Biotechnol.*, 2003, **21**, 1184–1191.
- 30 D. Mata, F. J. Oliveira, N. M. Ferreira, R. F. Araújo, A. J. S. Fernandes, M. A. Lopes, P. S. Gomes, M. H. Fernandes and R. F. Silva, *Nanotechnology*, 2014, **25**, 145602.
- 31 D. Mata, A. L. Horovistiz, I. Branco, M. Ferro, N. M. Ferreira, M. Belmonte, M. A. Lopes, R. F. Silva and F. J. Oliveira, *Mater. Sci. Eng., C*, 2014, **34**, 360–368.
- 32 L. F. Jaffe and R. Nuccitelli, *J. Cell Biol.*, 1974, **63**, 614–628.
- 33 C. Scheffey, *Rev. Sci. Instrum.*, 1988, **59**, 787–792.
- 34 B. Reid, R. Nuccitelli and M. Zhao, *Nat. Protoc.*, 2007, **2**, 661–669.
- 35 B. M. Isaacson and R. D. Bloebaum, *J. Biomed. Mater. Res., Part A*, 2010, **95**, 1270–1279.
- 36 J. Loza, E. Stephan, C. Dolce, R. Dziak and S. Simasko, *Calcif. Tissue Int.*, 1994, **55**, 128–133.
- 37 S. Jalota, S. B. Bhaduri and A. C. Tas, *J. Biomed. Mater. Res., Part A*, 2006, **78**, 481–490.
- 38 R. Cuscó, F. Guitián, S. d. Aza and L. Artús, *J. Eur. Ceram. Soc.*, 1998, **18**, 1301–1305.
- 39 S. Grimnes and G. Martinsen, *Bioimpedance and Bioelectricity Basics*, Academic Press, UK, 2008.
- 40 E. Czekanska, M. Stoddart, R. Richards and J. Hayes, *Eur. Cells Mater.*, 2012, **24**, 1–17.
- 41 J. Jansen, O. van der Jagt, B. Punt, J. Verhaar, J. van Leeuwen, H. Weinans and H. Jahr, *BMC Musculoskeletal Disord.*, 2010, **11**, 188.
- 42 M.-T. Tsai, W.-J. Li, R. S. Tuan and W. H. Chang, *J. Orthop. Res.*, 2009, **27**, 1169–1174.
- 43 P. T. O'Donnell, V. L. Collier, K. Mogami and S. I. Bernstein, *Genes Dev.*, 1989, **3**, 1233–1246.
- 44 J. E. Aubin and J. T. Triffitt, Mesenchymal stem cell and osteoblast differentiation, in *Principles of bone biology*, ed. J. P. Bilezikian, L. G. Raisz and G. A. Rodan, Academic Press, USA, 2002, vol. 1, pp. 59–81.
- 45 H. K. Datta, W. F. Ng, J. A. Walker, S. P. Tuck and S. S. Varanasi, *J. Clin. Pathol.*, 2008, **61**, 577–587.
- 46 K. Matsuo and N. Irie, *Arch. Biochem. Biophys.*, 2008, **473**, 201–209.
- 47 S. Giannona, I. Firkowska, J. Rojas-Chapana and M. Giersig, *J. Nanosci. Nanotechnol.*, 2007, **7**, 4–5.
- 48 S. Namgung, K. Y. Baik, J. Park and S. Hong, *ACS Nano*, 2011, **5**, 7383–7390.

- 49 I. Titushkin, S. Sun, J. Shin and M. Cho, *J. Biomed. Biotechnol.*, 2010, **2010**, 1–14.
- 50 S. Sun, Y. Liu, S. Lipsky and M. Cho, *FASEB J.*, 2007, **21**, 1472–1480.
- 51 I. Titushkin and M. Cho, *Biophys. J.*, 2007, **93**, 3693–3702.
- 52 S. E. Guggino, J. A. Wagner, A. M. Snowman, L. D. Hester, B. Sacktor and S. H. Snyder, *J. Biol. Chem.*, 1988, **263**, 10155–10161.
- 53 D. Chesnoy-Marchais and J. Fritsch, *J. Physiol.*, 1988, **398**, 291–311.
- 54 B. Z. Peterson, C. D. DeMaria and D. T. Yue, *Neuron*, 1999, **22**, 549–558.
- 55 M. Zayzafoon, *J. Cell. Biochem.*, 2006, **97**, 56–70.